Available online at www.sciencedirect.com

ScienceDirect

Ceramics International 40 (2014) 4963–4968

CERAMICS INTERNATIONAL

www.elsevier.com/locate/ceramint

Enhancement of temperature coefficient of resistivity in $La_{0.67}Ca_{0.33}MnO_3$ polycrystalline ceramics

Ji Ma[a], Yunqi Cai[a], Wenzhang Wang[a], Qi Cui[a], Mya Theingi[a,b], Hui Zhang[a], Qingming Chen[a,*]

[a]*Faculty of Materials Science and Engineering, Kunming University of Science and Technology, Kunming 650093, China*
[b]*Department of Chemistry, University of Yangon, Yangon 11181, Myanmar*

Received 27 August 2013; received in revised form 16 October 2013; accepted 22 October 2013
Available online 29 October 2013

Abstract

$La_{0.67}Ca_{0.33}MnO_3$ polycrystalline ceramics with high temperature coefficient of resistivity (TCR) have been synthesized by the sol–gel method at the sintering temperature of 1450 °C and in a sintering time range of 2 h–24 h. The micrographs of the ceramics reveal that the grains grow up from 2 μm to about 10 μm with increasing the sintering time. The optimization of the sintering time is found to be a simple and effective way to largely enhance the TCR values of the ceramics. The highest metal–insulator transition temperature T_p (272.5 K) and the largest TCR (21.4%) were obtained in the ceramic sintered for 12 h. The reduction of grain boundary and resistivity contributes to the enhancement of T_p and TCR values.

Keywords: Sol–gel; Sintering time; Electrical transport properties; $La_{0.67}Ca_{0.33}MnO_3$ ceramics

1. Introduction

The rare earth doped perovskite manganite $La_{1-x}Ca_xMnO_3$ has been intensively studied in the past decades since the colossal magnetoresistance (CMR) effect was observed in the material system [1–5]. It has a general chemical formula of ABO_3, in which Mn ions occupy the B-site at the center of the unit cell and are octahedrally coordinated by the oxygen ions. The La^{3+} and Ca^{2+} ions are distributed randomly over the A-sites in the crystal. With the variation in Ca concentration, the compound $La_{1-x}Ca_xMnO_3$ shows a rich phase diagram of ground state. At the ends of the doping level, $LaMnO_3$ is a tetragonal layered antiferromagnet (AFM) and $CaMnO_3$ is a G-type AFM with opposite spin orientations for nearest-neighbor Mn^{4+} spins [6,7]. At Ca concentration of 0.2–0.5, where CMR effect is observed, the material shows a paramagnetic-insulator to ferromagnetic-metal transition with the change in the ambient temperature [2]. It is accepted that double exchange and Jahn–Teller effect are attributed to the ferromagnetic metallic state and paramagnetic insulator state, respectively [8,9]. In the doping process, the substitution of trivalent La^{3+} by divalent Ca^{2+} leads to the decrease in the ratio of Mn^{3+} to Mn^{4+} ions. The variations in the $Mn^{3+}3O3Mn^{4+}$ bond length and bond angle change the electron hopping and carriers localization and therefore determine the electronic and magnetic transport properties of the materials [10].

Recently, a lot of researches have been focused on the heterojunction and sandwich structure of $La_{1-x}Ca_xMnO_3$ thin films (i.e. LCMO/LSMO [11], $La_{2/3}Ca_{1/3}MnO_3/YBa_2Cu_3O_7$ [12], LCMO/STO/YBCO [13]) due to their unusual transport properties. In terms of polycrystalline ceramic, the low field magnetoresistance (LFMR) has attracted considerable efforts since the low field limits the practical application of the CMR effect [14–16]. Besides the CMR and LFMR effects, electro-resistance (ER) effect has also triggered many researches on its potentiality as an alternative for CMR in industrial application [13,17,18].

Since the highest Curie temperature (T_C) is acquired at $x \approx 0.33$, and CMR usually reaches its maximum around T_C,

*Corresponding author. Tel.: +86 871 65109292; fax: +86 871 65107922.
E-mail addresses: majimacao@163.com (J. Ma), chqm99@yahoo.com (Q.M. Chen).

0272-8842/$ - see front matter © 2013 Elsevier Ltd and Techna Group S.r.l. All rights reserved.
http://dx.doi.org/10.1016/j.ceramint.2013.10.105

the composite $La_{0.67}Ca_{0.33}MnO_3$ becomes the most popular subject in this kind of material system [19–21]. The development of highly sensitive bolometers at room temperature requires materials with high T_p and TCR values [22]. In $La_{1-x}Ca_xMnO_3$ system, the optimal doping level for obtaining the highest insulator–metal transition temperature (T_p) and paramagnetic–ferromagnetic transition temperature (T_C) is around $x=0.33$. The largest TCR value which in general is less than 10% is usually obtained at Ca doping level of 0.33 as well. Double doping with Ca and Sr can further enhance the T_p value, while the TCR value will decrease at the same time [23]. In this paper, we have prepared the $La_{0.67}Ca_{0.33}MnO_3$ polycrystalline ceramics by calcinating the precursor powders at a low temperature (500 °C) and sintering the ceramics at a high temperature (1450 °C) according to our previous works. By changing the sintering time from 2 h to 24 h, we obtained the largest T_p of 272.5 K and TCR value of 21.4% at the sintering time of 12 h. To characterize the sintering time effects on the transport properties, the low-temperature behavior ($T < T_p$) and high-temperature behavior ($T > T_p$) have been fitted by using a $T^{4.5}$ power law and the variable-range hopping model, respectively.

2. Experiments

Polycrystalline $La_{0.67}Ca_{0.33}MnO_3$ (LCMO) ceramics were synthesized by a simple sol–gel method with citric acid as the chelating agent [24]. Our previous work has demonstrated that enlarging the difference between the calcination and sintering temperature is an efficient way to improve the TCR value [25]. In addition, the sintering time and sintering temperature are also very important for the grain growth, which has a strong influence on the transport properties of ceramics [26]. According to our experiments, the precursor LCMO powders were calcinated at a low temperature of 500 °C for 12 h. The obtained black powders were grinded and sintered at a high temperature of 1450 °C for 2 h, 8 h, 12 h, 16 h and 24 h, respectively.

The structures and phases of the samples were examined by X-ray diffraction (XRD) with the Cu K_α radiation at room temperature. The surface morphologies of the ceramics were characterized by scanning electron microscopy (SEM). The resistance of the samples was measured by using the four probe method in the temperature range of 300–100 K.

3. Results and discussion

XRD patterns of the LCMO polycrystalline ceramics sintered for different time are shown in Fig. 1. All the samples have a single phase with the perovskite structure. It indicates that the sintering time has a negligible influence on the formation of LCMO phase, perhaps because the sintering temperature is high enough.

The temperature dependence of resistivity of the LCMO samples is shown in Fig. 2. The TCR (TCR=$(1/\rho)(d\rho/dT)$ 100%) values were obtained from the $\rho(T)$ data and shown in Fig. 3. All the ceramics sintered over 8 h show the sharp

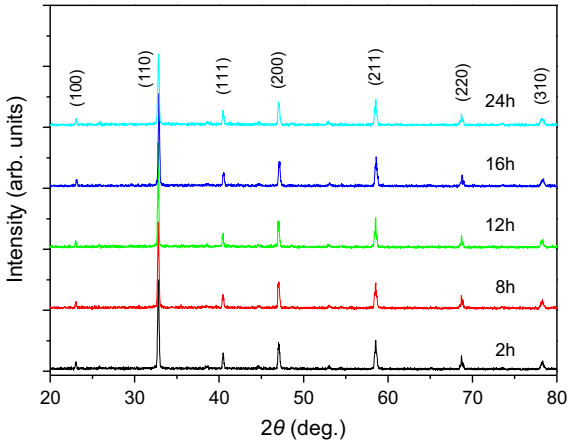

Fig. 1. XRD patterns of LCMO ceramics sintered at 1450 °C for different time.

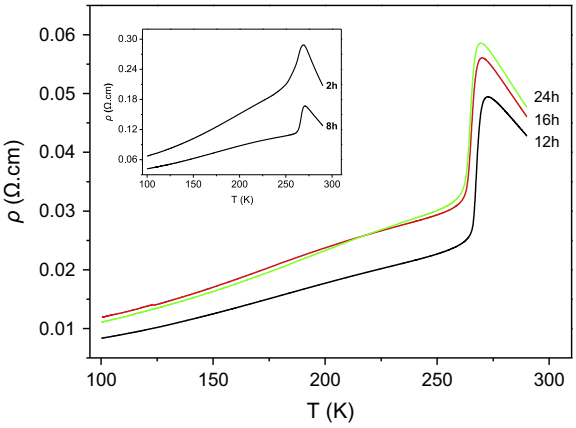

Fig. 2. Temperature dependence of resistivity of the LCMO ceramics sintered for different time.

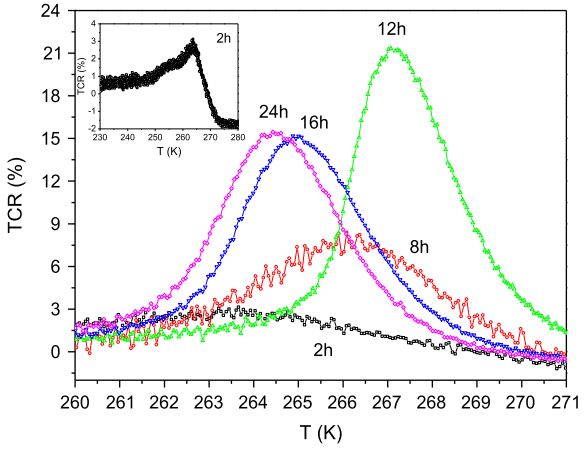

Fig. 3. TCR curves of the LCMO ceramics. Inset shows the enlarged view of the ceramic sintered for 2 h.

metal–insulator transition at the temperature $T_p \approx 270$ K. The physical properties, such as T_p, electrical resistivity and relative density of the samples change with the sintering time increasing. These relationships are plotted in Fig. 4. It can be seen that both T_p and TCR values increase at first and then

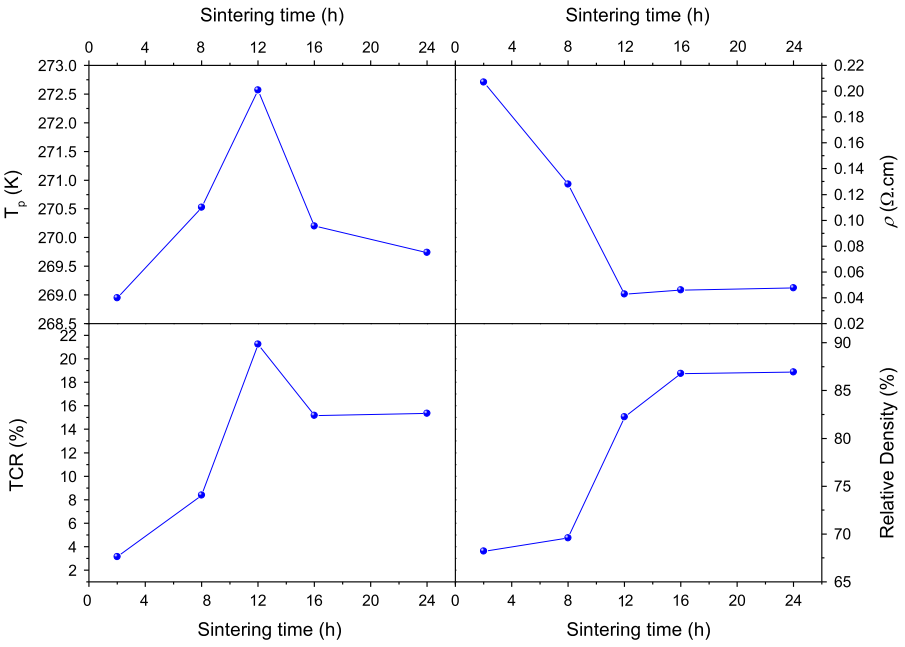

Fig. 4. Dependence of T_p, TCR, ρ and relative density of the LCMO ceramics with the sample sintering time.

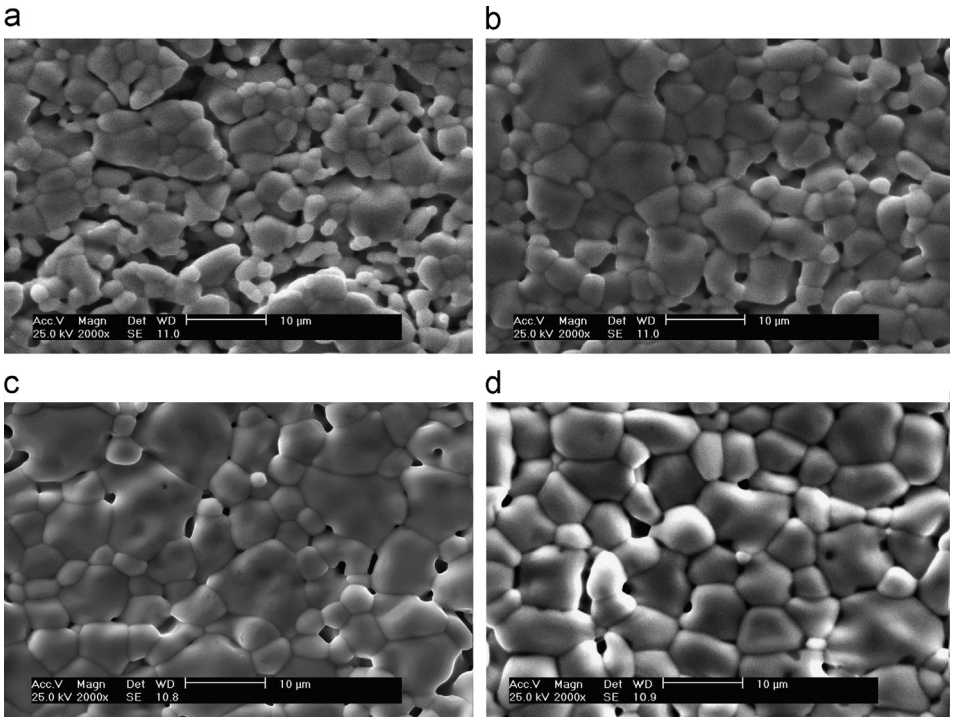

Fig. 5. SEM micrographs of LCMO ceramics sintered for (a) 2 h, (b) 8 h, (c) 12 h and (d) 24 h.

decrease. For the ceramic sintered for 2 h, a broad metal–insulator transition appears at $T_p = 269.0$ K with a small TCR value of 3.0%. For the sample sintered for 12 h, the values of T_p and TCR reach to the maximum at the same time as 272.5 K and 21.4%, respectively. The resistivity of the ceramics first decreases with the increase in the sintering time and reach a minimum with sintering time of 12 h. While the sintering time keeps increasing, the resistivity of the material increases slightly. The relative density (defined as the ratio between the calculated practical density and theoretical density of bulk $La_{0.67}Ca_{0.33}MnO_3$) of the ceramics increases fast when extending the sintering time, and changes little above 16 h.

It is well known that the doping level of Ca and the oxygen content significantly influence the magnetic and electronic properties of the material as the Mn^{3+}/Mn^{4+} ratio changes. The occurrence of oxygen vacancies would weaken the hopping of e_g electrons between Mn^{3+} and Mn^{4+}, which would reduce the density of charge carriers and result in the

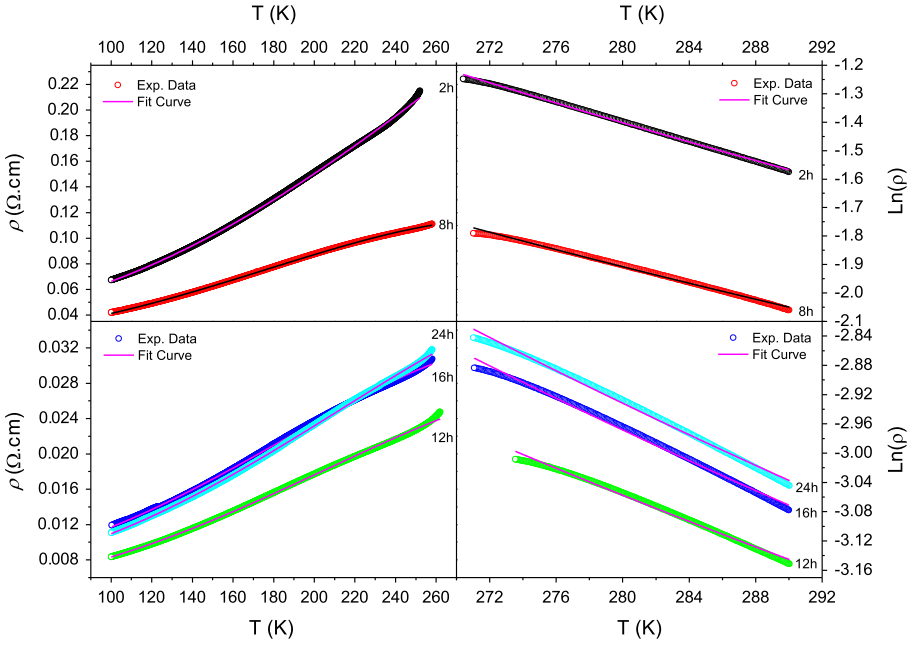

Fig. 6. Fits of low and high temperature resistivity of LCMO ceramics to the expression $\rho(T)=\rho_0+\rho_2T^2+\rho_{4.5}T^{4.5}$ and $\rho(T)=\rho_0\exp(T_0/T)^{1/4}$, respectively.

decrease in T_p and broadening of the resistivity peak [27]. On the other hand, T_p is supposed to decrease with the decrease in grain size. The total resistivity of polycrystalline is assumed to originate from bulk grain resistivity and the intergrain boundaries resistivity [28]. The grain boundary acts as a region of enhanced scattering for the conduction electrons and increases the total resistivity. Base on the above analysis, the present results in Fig. 4 can be explained. The sintering time has a direct influence on the grain growth. The oxygen stoichiometry decreases as the sintering time decreases, which results in a broader resistivity peak, a higher resistivity value and a lower metal–insulator transition T_p. For a longer sintering time, the oxygen content increases and the grain boundaries decreases, at 12 h, T_p and TCR reach the largest at the same time as the deficiencies is the least. But further increasing the sintering time will lead to the increase of the oxygen vacancies and the deficiencies at the grain boundaries. Therefore, the electrical properties will no longer be improved.

As shown in Fig. 5, the increase in the sintering time significantly promotes the grain growth, For a short sintering time of 2 h (Fig. 5(a)), the grain size is small (2–3 μm) and the grains agglomerate obviously. Large number of weak-links appear. A lot of large pores exist among the grains and particles, inducing material inhomogeneity and leading to a large resistivity and small density of the ceramics. Consequently, the metal–insulator transition region is broad and the TCR is very small. With the increase in the sintering time, the grains have more time to grow up and the pores can be released gradually. The reduction in the weak-links also occurs along with the grain growth. The decrease in grain boundaries and pores then improves the electric conductivity and homogeneity of the sample. Therefore, the T_p and TCR values are enhanced largely. After sintered for 8 h (Fig. 5(b)), many grains grow up to about 5 μm, while there are still a number of small grains (2–3 μm). Both the small and large grains continue growing up for 12 h sintering time (Fig. 5(c)). It contributes to the formation of strong intergrain connectivity and enhances electrical transport. The further decrease in grain boundaries and a possible increase in oxygen in the lattice enhance the T_p and TCR. For the sample sintered for 24 h (Fig. 5 (d)), almost all the grains have a similar size about 8–10 nm, but its electrical properties is not the best. We think that a too long sintering time may induce more disorders and defects between the grains. Therefore, a slight increase in the resistivity and decrease in the T_p and TCR were observed.

In Fig. 6, we plot the measurement results of the resistivity and the corresponding fitting curves of the LCMO ceramics at low temperature (100–260 K) and high temperature (270–290 K), respectively. The electrical transport behavior at low temperature ($T<T_p$) can be well fitted using the formula: $\rho(T)=\rho_0+\rho_2T^2+\rho_{4.5}T^{4.5}$ [2,29] where ρ_0 is the residual resistivity due to domain boundaries and other temperature-independent scattering, ρ_2T^2 represents the electron–electron scattering, $\rho_{4.5}T^{4.5}$ is attributed to the electron–magnon or two-magnon scattering process. For all the samples, the fit provides an excellent approximation of the experimental data. All the parameters are found to decrease first with increasing the sintering time, reach a minimum at 12 h, and then increase. The decrease in resistivity can be attributed to the reduction in grain boundary and increase in grain size with the increasing in sintering time, since the grain size and mechanical connection between grains play an important role in the electronic conduction. As a result, the scattering processes are suppressed and ρ_0, ρ_2 and $\rho_{4.5}$ change with the variation in the grain size.

In the paramagnetic phase ($T>T_p$), there are three possible mechanisms to describe the conduction behavior: the thermally activated model ($\rho(T)=\rho_0\exp(E_A/k_BT)$) [30], the nearest neighbor hopping model ($\rho(T)=AT\exp(E_A/k_BT)$) and the variable range hopping model (VRH) ($\rho(T)=\rho_0\exp(T_0/T)^{1/4}$) [31–33].

In our experiments, the VRH model is the best one to fit our data for all samples. The residual resistivity ρ_0 and characteristic VRH temperature T_0 values are found to decrease first and then increase with increasing the sintering time. The minimum values are obtained at 12 h. Since T_0 is related to the localization length, the higher T_0 value implies an increase in the bending of Mn–O–Mn bond which decreases the localization length and thus the carrier mobility is reduced [34]. Therefore the observed tendency is due to the fact that the increase in grain size and changes in the amount of grain boundary enhance the localization length and result in a large change in resistivity.

4. Conclusions

We have investigated the effects of sintering time on the structures, morphologies and electrical transport properties of polycrystalline $La_{0.67}Ca_{0.33}MnO_3$ ceramics. The results show that it is possible to largely enhance the TCR value by appropriate sintering schedule, and processing and tailoring material of this composition may yield better performance for bolometric device application based on insulator–metal transportation. With the sintering time increased from 2 h to 24 h, the grains grow up and the relative density of the ceramic increase. The T_p and TCR values increase at first and then decrease. The largest TCR (21.4%) with the highest T_p (272.5 K) was obtained in the sample sintering for 12 h, which can be attributed to the least grain boundary and deficiencies, and the smallest resistivity of the sample. In the ferromagnetic state ($T < T_p$), the $\rho(T)$ curves of the ceramics can be well fitted using a $T^{4.5}$ power law. In the paramagnetic state ($T > T_p$), the $\rho(T)$ characteristics can be explained using the variable range hopping model.

Acknowledgments

This work is supported by the National Science Foundation of China (50902062) and Key Programme of Kunming University of Science and Technology (KKZ1200927002).

References

[1] S. Jin, T.H. Tiefel, M. McCormack, R.A. Fastnacht, R. Ramesh, L.H. Chen, Thousandfold change in resistivity in magnetoresistive La–Ca–Mn–O films, Science 264 (1994) 413–415.
[2] P. Schiffer, A.P. Ramirez, W. Bao, S-W. Cheong, Low temperature magnetoresistance and the magnetic phase diagram of $La_{1-x}Ca_xMnO_3$, Phys. Rev. Lett. 75 (1995) 3336–3339.
[3] J. Feng, B. Xiao, C.L. Wan, Z.X. Qu, Z.C. Huang, J.C. Chen, R. Zhou, W. Pan, Electronic structure, mechanical properties and thermal conductivity of $Ln_2Zr_2O_7$ (Ln=La, Pr, Nd, Sm, Eu and Gd) pyrochlore, Acta Mater. 59 (2011) 1742.
[4] J. Feng, B. Xiao, R. Zhou, W. Pan, Electronic and magnetic properties of double perovskite slab–rocksalt layer rare earth strontium aluminates natural superlattice structure, J. Appl. Phys. 113 (2013) 143907–143910.
[5] E. Restrepo-Parra, C.D. Salazar-Enríquez, J. Londoño-Navarro, J. F. Jurado, J. Restrepo, Magnetic phase diagram simulation of $La_{1-x}Ca_xMnO_3$ system by using Monte Carlo, Metropolis algorithm and Heisenberg model, J. Magn. Magn. Mater. 323 (2011) 1477–1483.
[6] J. van den Brink, P. Horsch, F. Mack, A.M. Oleś, Orbital dynamics in ferromagnetic transition-metal oxides, Phys. Rev. B 59 (1999) 6795–6805.
[7] J.B. Goodenough, Theory of the role of covalence in the perovskite-type manganites [La, M(II)]MnO_3, Phys. Rev. 100 (1955) 564–573.
[8] C. Zener, Interaction between the d shells in the transition metals, Phys. Rev. 81 (1951) 440–444.
[9] V.L. Moruzzi, P.M. Marcus, Magnetism in bcc 3d transition metals: onset and approach to the Hund's-rule limit, Phys. Rev. B, 38, , 1988, p. 1613–1620.
[10] C.D. Hu, Low-temperature resistivity of double-exchange interaction systems, Phys. Rev. B 66 (2002) 132404-4.
[11] T. Nurgaliev, U. Topal, B. Blagoev, E. Mateev, Magnetic Properties of LCMO/LSMO Thin Films on LAO and ALO Substrates, J. Superconductivity Novel Magn. 25 (2012) 2495–2498.
[12] S.R. Giblin, J.W. Taylor, J.A. Duffy, M.W. Butchers, C. Utfeld, S.B. Dugdale, T. Nakamura, C. Visani, J. Santamaria, Measurement of magnetic exchange in ferromagnet-superconductor $La_{2/3}Ca_{1/3}MnO_3$/$YBa_2Cu_3O_7$ bilayers, Phys. Rev. Lett. 109 (2012) 137005-5.
[13] S.A. Fedoseev, A.V. Pan, O.V. Shcherbakova, S.X. Dou, Electroresistance and magnetoresistance effects in superconductor–insulator–ferromagnet hybrid structures, Phys. C: Superconductivity Appl. 479 (2012) 143–146.
[14] S.D. Bhame, J.-F. Fagnard, M. Pekala, P. Vanderbemden, B. Vertruyen, $La_{0.7}Ca_{0.3}MnO_3$/Mn_3O_4 composites: does an insulating secondary phase always enhance the low field magnetoresistance of manganites?, J Appl. Phys. 111 (2012) 063905-4.
[15] D.G. Li, Z.H. Peng, Y.H. Xiong, L.J. Li, Z.L. Liu, C.S. Xiong, Magnetic and electrical transport properties of Er_2O_3-doped $La_{0.7}Ca_{0.3}MnO_3$ composites, J. Superconductivity Novel Magn. 25 (2012) 1523–1527.
[16] P.T. Phong, N.V. Khiem, N.V. Dai, D.H. Manh, L.V. Hong, N.X. Phu, Low-field magnetoresistance of $(1-x)La_{0.7}Ca_{0.3}MnO_3+xAg$ composites, J. Alloys Compd. 484 (2009) 12–16.
[17] I.G. Deac, I. Balasz, Electroresistance, magnetocapacitance and magnetotransport properties of $La_{0.55}Ca_{0.45}MnO_3$/$BaTiO_3$ composite, Mater. Chem. Phys. 136 (2012) 850–857.
[18] L.P. Chen, J. Gao, Current induced metastable states and abnormal electroresistance effect in epitaxial thin films of $La_{0.8}Ca_{0.2}MnO_3$, Solid State Commun. 151 (2011) 1293–1295.
[19] X.R. Zhu, Z.G. Zhu, C. Chen, H.L. Shen, K. Tsukamoto, T. Yanagisawa, M. Okutomi, N. Higuchi, Hysteresis and vertical anisotropy of magnetoresistance in $La_{0.67}A_{0.33}MnO_z$ (A=Ca, Sr) polycrystalline films deposited on amorphous quartz substrates, Ceram. Int. 39 (2013) 9025–9031.
[20] G. Venkataiah, V. Prasad, P. Venugopal Reddy, Influence of A-site cation mismatch on structural, magnetic and electrical properties of lanthanum manganites, J. Alloys Compd. 429 (2007) 1–9.
[21] Y.W. Liu, Z.H. Yang, H.L. Yang, Y.L. Xie, S. K., B. Chen, Q.F. Zhan, R.W. Li, Anisotropic magnetoresistance in epitaxial $La_{0.67}(Ca_{1-x}Sr_x)_{0.33}MnO_3$ films, J. Appl. Phys. 113 (2013) 17C722-3.
[22] Ravi Bathe, K.P. Adhi, S.I. Patil, G. Marest, B. Hannoyer, S.B. Ogale, Silver ion implantation in epitaxial $La_{2/3}Ca_{1/3}MnO_3$ thin films: large temperature coefficient of resistance for bolometric applications, Appl. Phys. Lett. 76 (2000) (2104–3).
[23] T.D. Thanh, L.H. Nguyen, D.H. Manh, N.V. Chien, P.T. Phong, N.V. Khiem, L.V. Hong, N.X. Phuc, Structural, magnetic and magnetotransport behavior of $La_{0.7}Sr_xCa_{0.3-x}MnO_3$ compounds, Phys. B: Condens. Matter 407 (2012) 145–152.
[24] J. Ma, M. Theingi, H. Zhang, W.Z. Wang, J.H. Yi, Q.M. Chen, Structural and electrical characterization of $La_{0.72}Ca_{0.28}MnO_3$ ceramic and thin films, Appl. Surf. Sci. 264 (2013) 225–228.
[25] J. Ma, M. Theingi, Q.M. Chen, W.Z. Wang, X. Liu, H. Zhang, Influence of synthesis methods and calcination temperature on electrical properties of $La_{1-x}Ca_xMnO_3$ (x=0.33 and 0.28) ceramics, Ceram. Int. 39 (2013) 7839–7843.
[26] L. Lei, Z. Fu, J. Zhang, H. Wang, K. Niihara, Low field magnetoresistance of $La_{0.7}Ca_{0.3}MnO_3$ ceramics fabricated by fast sintering process, J. Alloys Compd. 530 (2012) 164–168.
[27] Y.Kalyana Lakshmi, P.Venugopal Reddy, Influence of silver doping on the electrical and magnetic behavior of $La_{0.7}Ca_{0.3}MnO_3$ manganites, Solid State Sci. 12 (2010) 1731–1740.

[28] N. Zhang, W. Ding, W. Zhong, D. Xing, Y. Du, Phys. Rev. B 56 (1997) 8138–8142.
[29] G.M. Zhao, H. Keller, W. Prellier, D.J. Kang, Bulk experimental evidence of half-metallic ferromagnetism in doped manganites, Phys. Rev. B 63 (2001) 172411–172414.
[30] X.W. Cao, J. Fang, K.B. Li, Electrical transport properties in magnetoresistive $La_{0.67}Ca_{0.33}MnO_3$ thin film, Solid State Commun. 115 (2000) 201–205.
[31] G. Jeffrey Snyder, Ron Hiskes, Steve DiCarolis, M.R. Beasley, T. H. Geballe, Electrical transport properties in magnetoresistive $La_{0.67}Ca_{0.33}MnO_3$ thin film, Solid State Commun. 115 (2000) 201–205.
[32] M. Viret, L. Ranno, J.M.D. Coey, Magnetic localization in mixed-valence manganites, Phys. Rev. B 55 (1997) 8067–8070.
[33] M. Ziese, C. Srinitiwarawong, Polaronic effects on the resistivity of manganite thin films, Phys. Rev. B 58 (1998) 11519–11525.
[34] J. Fontcuberta, B. Martinez, A. Seffar, S. Pinol, J.L. Garcia-Munoz, X. Obradors, Colossal magnetoresistance of ferromagnetic manganites: structural tuning and mechanisms, Phys. Rev. Lett. 76 (1996) 1122–1125.